

## **Table and Figure Captions**

**Table 1** Optimized material parameters obtained for a homogeneous, exponential, transversely isotropic model of the heart wall and the measured pressures at which experimental displacements were analyzed.

**Table 2** Optimized material parameters obtained for a model of the heart wall which consisted of an exponential, transversely isotropic myocardium and separate isotropic, exponential epicardium. The experimental displacements and pressures were identical to those in Table 1.

**Figure 1** Overview of the method for optimizing material properties using the epicardial suction. Epicardial suction is applied to a site on the LV. Geometry MR images are used to create an FE model that matches the experimental geometry and location of the suction cup. Measured pressures are used to define the loading for the FE model. Deformed and undeformed tag point locations are used to determine displacements. FE predicted displacements are interpolated from the FE model solution using the deformed tag point locations. At each iteration, the optimization algorithm solves forward FE problem and calculates the sum of squares of the difference between predicted and measured displacements at all data points. Material parameters in the constitutive relation used in the FE model are adjusted iteratively to minimize the sum of squares objective function.

**Figure 2** Experiment setup, showing: (1) isolated arrested heart in cold saline solution; (2) suction cup; (3) vacuum applied continuously in narrow channel surrounding orifice; (4) servopump; (5) suction pressure measurement; (6) holding fixture and MR orbit coil (cross-hatched). A clamp holding the suction cup in position has been omitted for clarity.

**Figure 3** Suction cup with concave surface of non-uniform curvature. The surface was contoured to approximately match the radii of curvature of the lateral free wall of the canine LV.

**Figure 4** Image planes for MR tagging. In order to acquire a 3-D deformation field, five image sequences were obtained in two orthogonal directions with image planes parallel to the walls of the suction cup. Image planes are approximately aligned with the long and short axes of the heart.

**Figure 5** MR tagged images through center of suction cup for experiment 06. (A) and (B): Undeformed short and long-axis images. (C) and (D): Images acquired at  $t = 60$  ms, suction pressure = 2.3 kPa. (E) and (F): Images acquired at  $t = 105$  ms, suction pressure = 3.2 kPa.

**Figure 6** Deformed shape plots of FE solution (Exp. 06) with optimized homogeneous material parameters at suction pressure of 3.2 kPa, corresponding to Figure 5E and 5F. (A) Short-axis view through center of suction cup (B) Long-axis view through center of suction cup.

**Figure 7** Normal (A) and shear (B) strain components as a function of transmural position in FE elements through center of suction cup. (C) Radial–circumferential shear strains in elements through the center of suction cup and to the anterior and posterior of center elements. (D) Radial–longitudinal shear strains in elements through the center of suction cup, and in elements toward the apex and base. All values were predicted from the FE model for experiment 06 using optimized material parameters at experimental pressure of 3.2 kPa as shown in Figure 6.

**Figure 8** Transmural variation in strain components in FE model of passive LV filling computed at 1 kPa cavity pressure. Lagrangian strain components referred to cardiac coordinates for five experiments were computed at the central gauss point of midventricular elements. Results shown are mean values with one-sided error bars of 1 SD for the model assuming homogeneous, transversely isotropic heart wall (open circles) and transversely isotropic myocardium and isotropic epicardium (open squares). Closed circles with error bars ( $\pm 1$  SD) represent experimental data of Omens et al. [10] on the anterior wall of the LV at midventricle at the same cavity pressure.

**Table 1**

Experiment	Pressures Analyzed (kPa)	Number of Data Points	Final Values of:				Mean Disp. Error (cm)
			$C$	$b_f$	$b_t$	$b_{fs}$	
01	0.84, 2.10, 3.58	394	0.3913	75.4109	33.8617	11.4987	0.018
03	1.10, 2.04, 2.94	407	1.0173	77.4928	8.0161	3.1216	0.018
04	0.84, 2.39, 3.20	400	0.7476	39.5292	6.1735	5.6649	0.022
06	0.79, 2.31, 3.17	371	0.3047	49.8868	11.1146	14.6322	0.027
07	0.80, 1.81, 3.48	316	0.1008	93.0273	61.6131	73.1017	0.022

**Table 2**

Experiment	Final Values of:						Mean Disp. Error (cm)
	$C_{myo}$	$b_f$	$b_t$	$b_{fs}$	$C_{epi}$	$b_{epi}$	
01	1.0543	31.1587	3.7345	3.6864	3.1421	44.1244	0.016
03	1.1432	70.8788	3.0269	2.0001	1.9891	25.0824	0.017
04	0.8759	13.6637	2.4250	2.9397	5.5866	15.5139	0.020
06	0.3595	53.4451	5.7746	10.1587	0.7122	21.7263	0.026
07	0.9897	10.2389	0.6979	3.7499	0.6468	95.2716	0.021

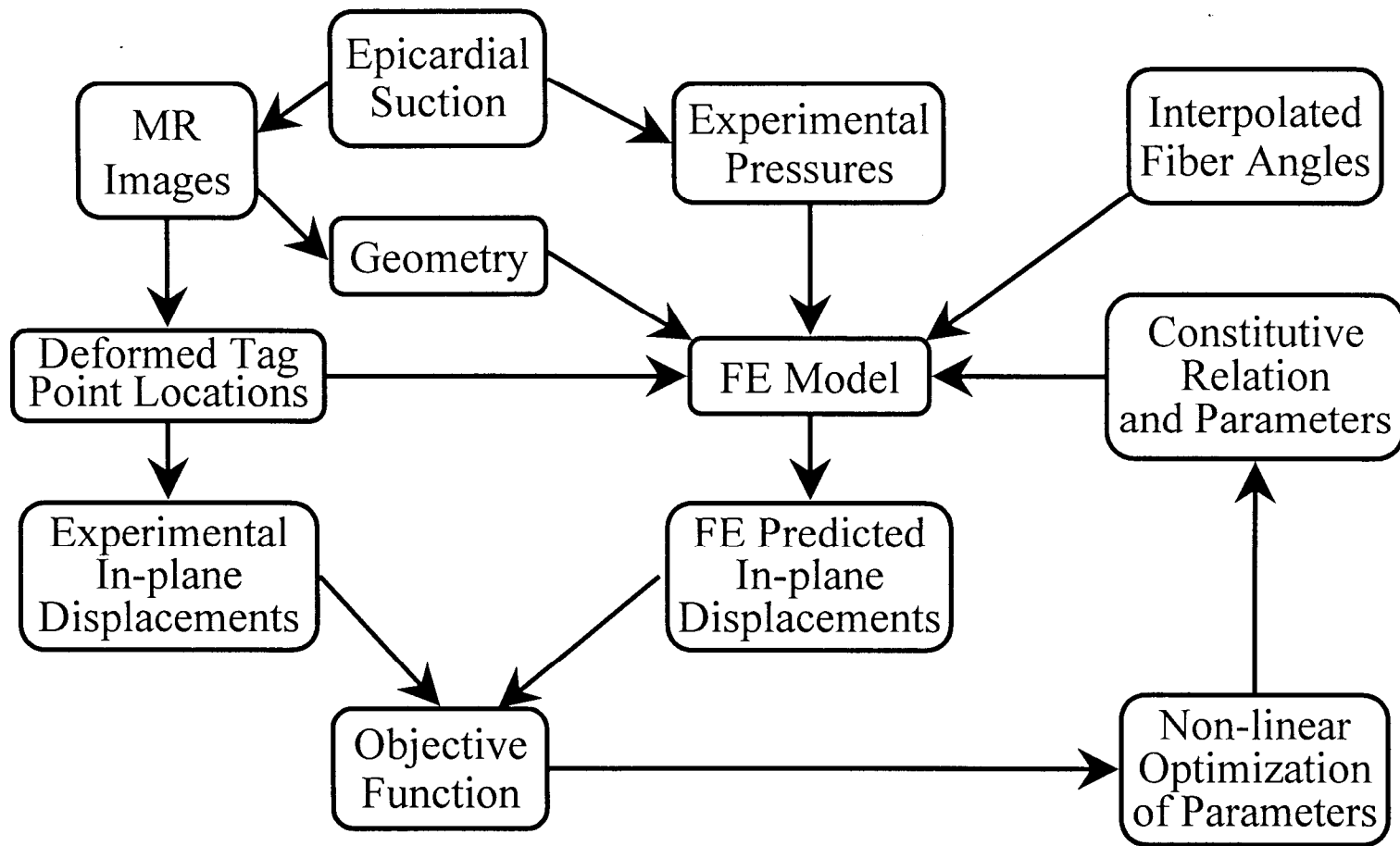


Figure 1, Okamoto et al.

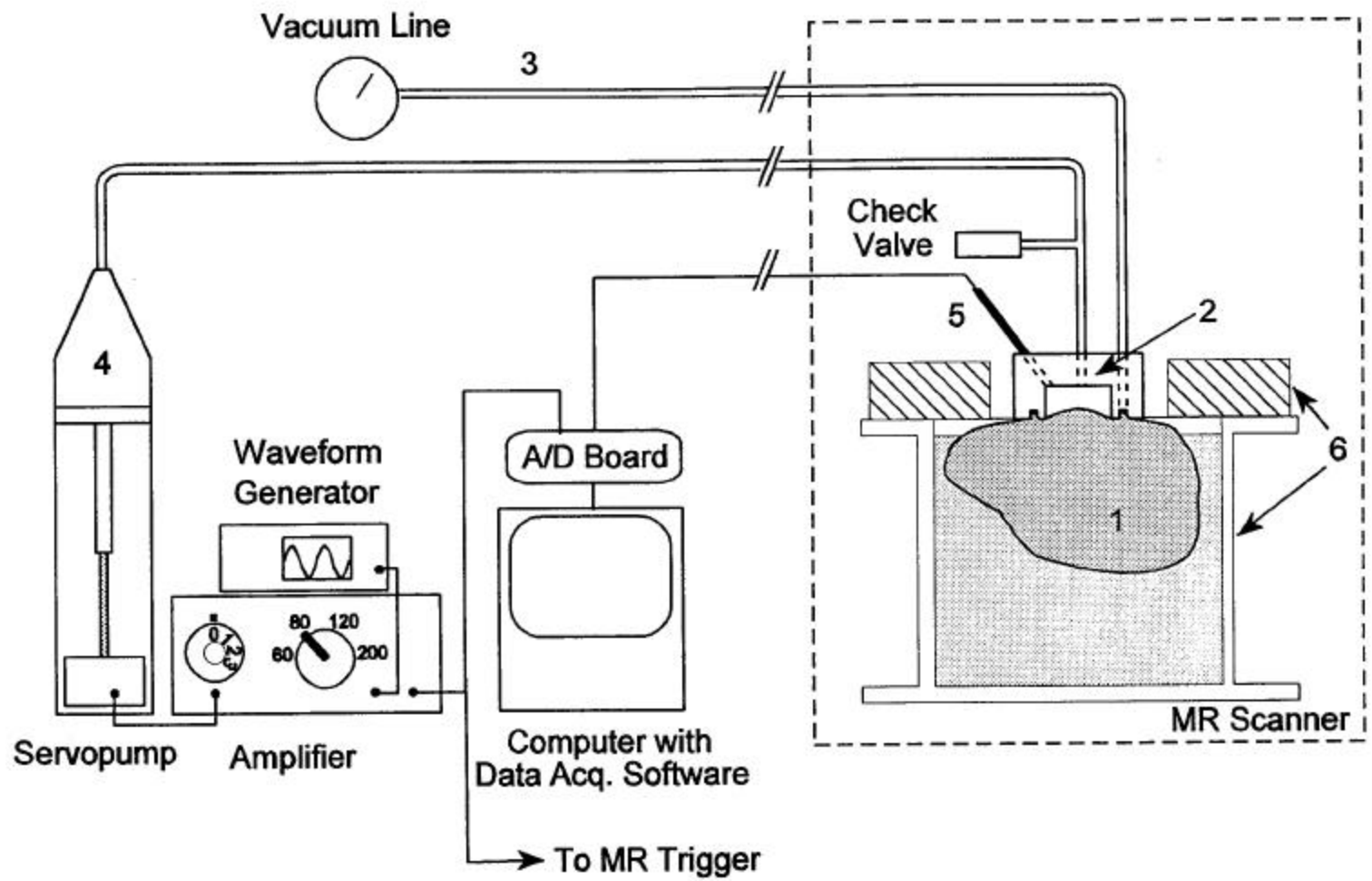


Figure 2, Okamoto et al.

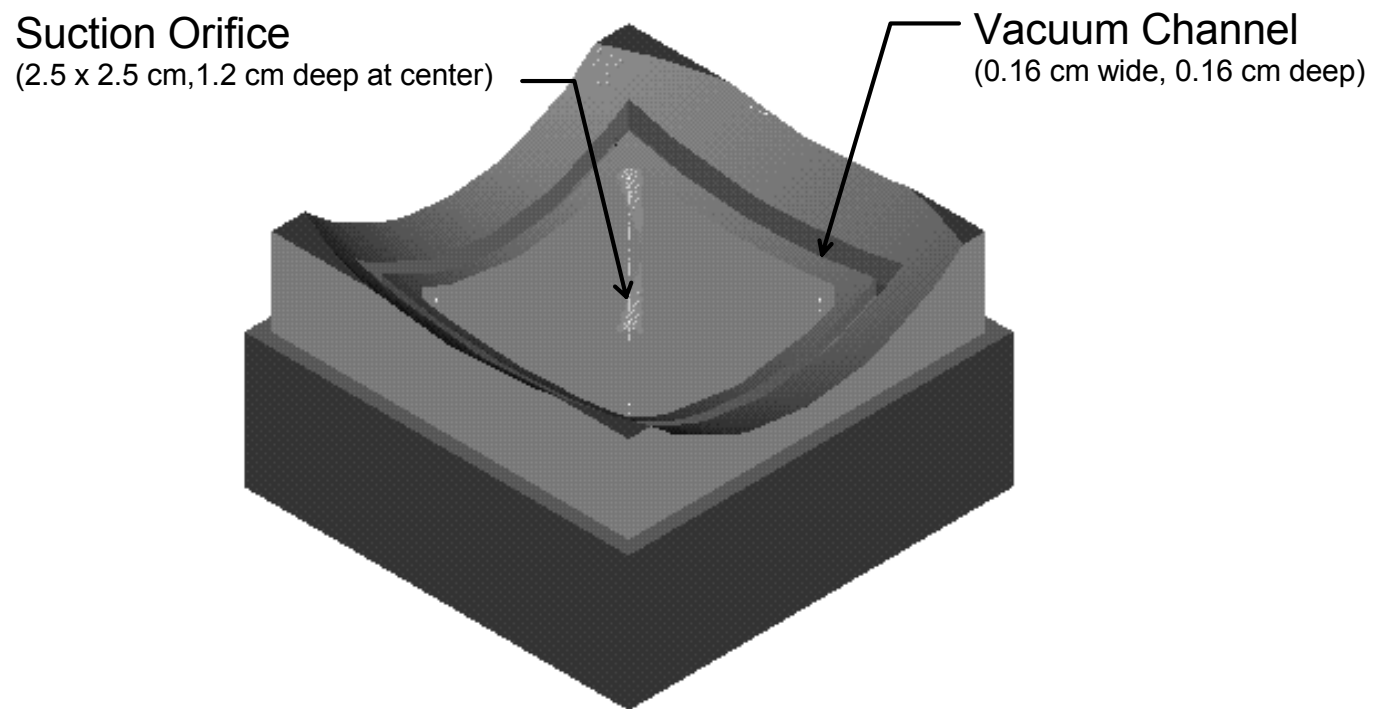
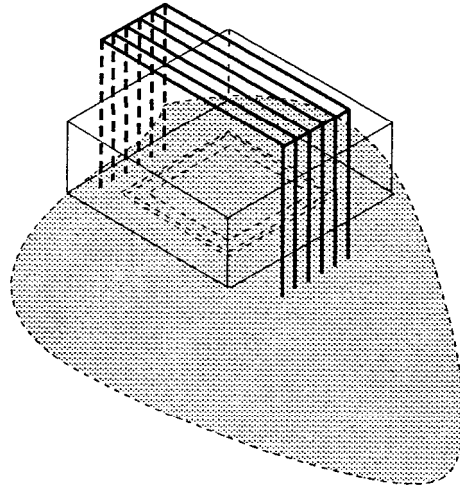
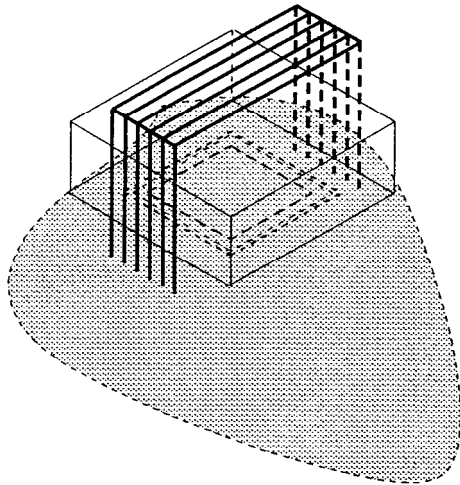


Figure 3, Okamoto et al.



Long Axis



Short Axis

Figure 4, Okamoto et al.

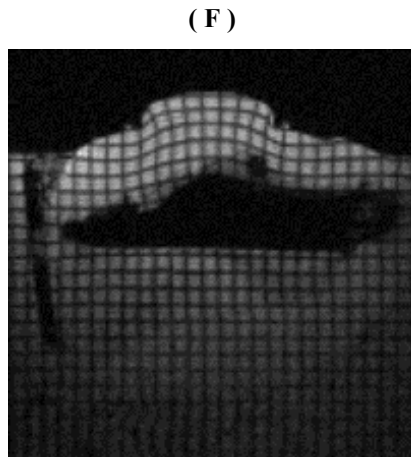
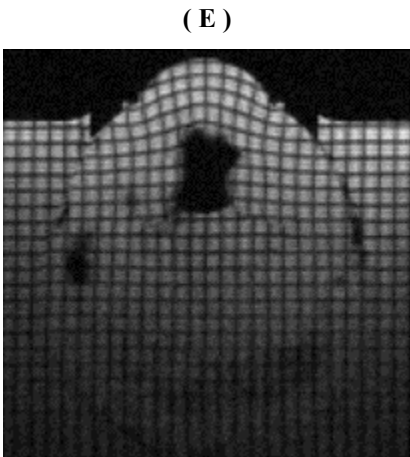
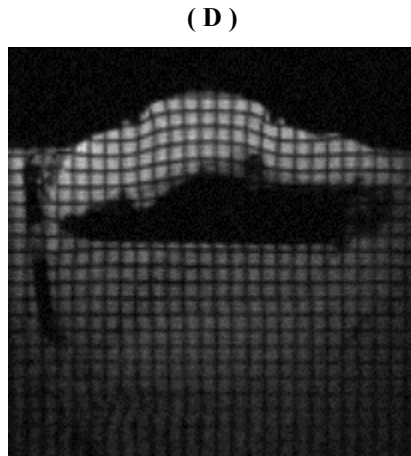
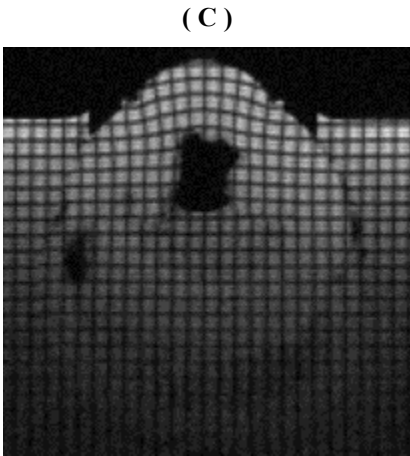
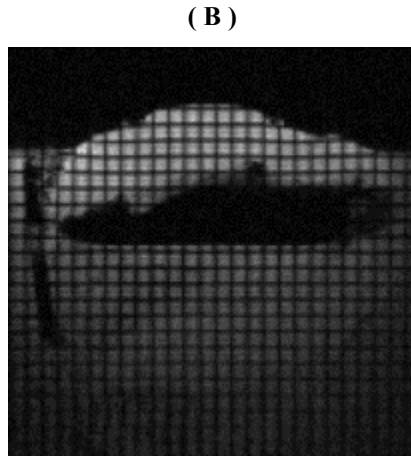
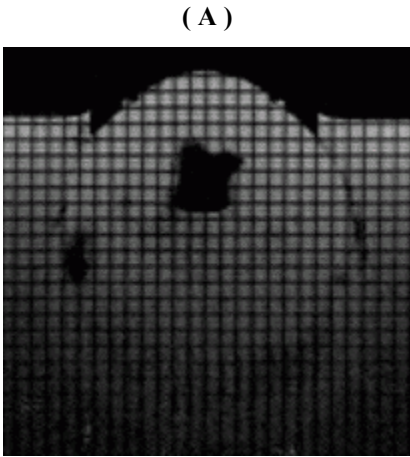
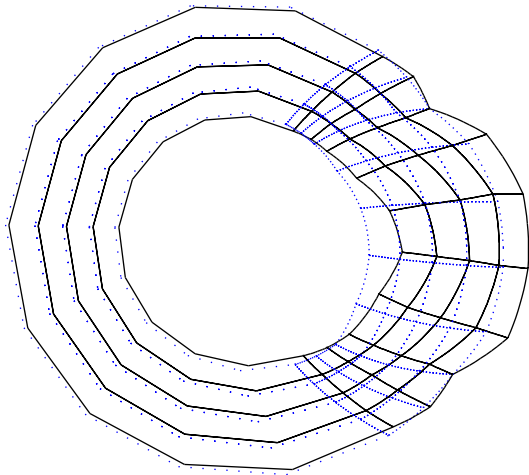


Figure 5, Okamoto et al.

(A)



(B)

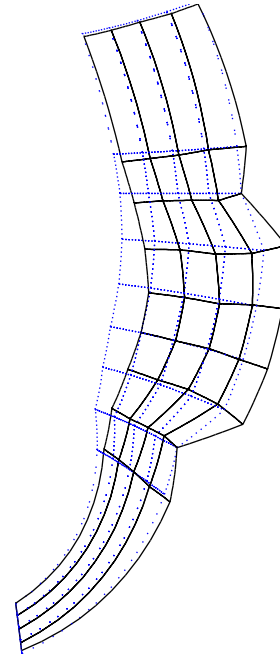


Figure 6, Okamoto et al.

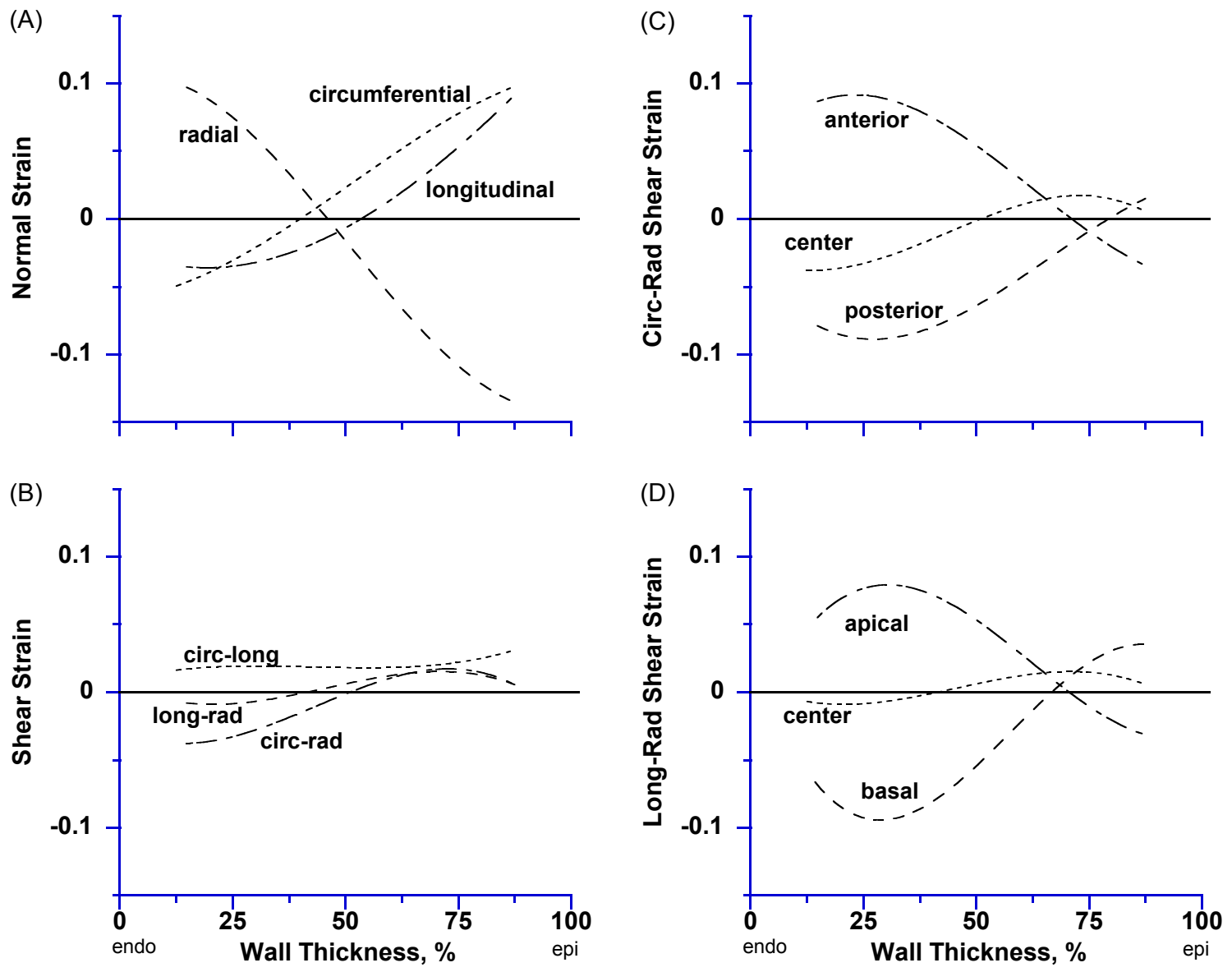


Figure 7, Okamoto et al.

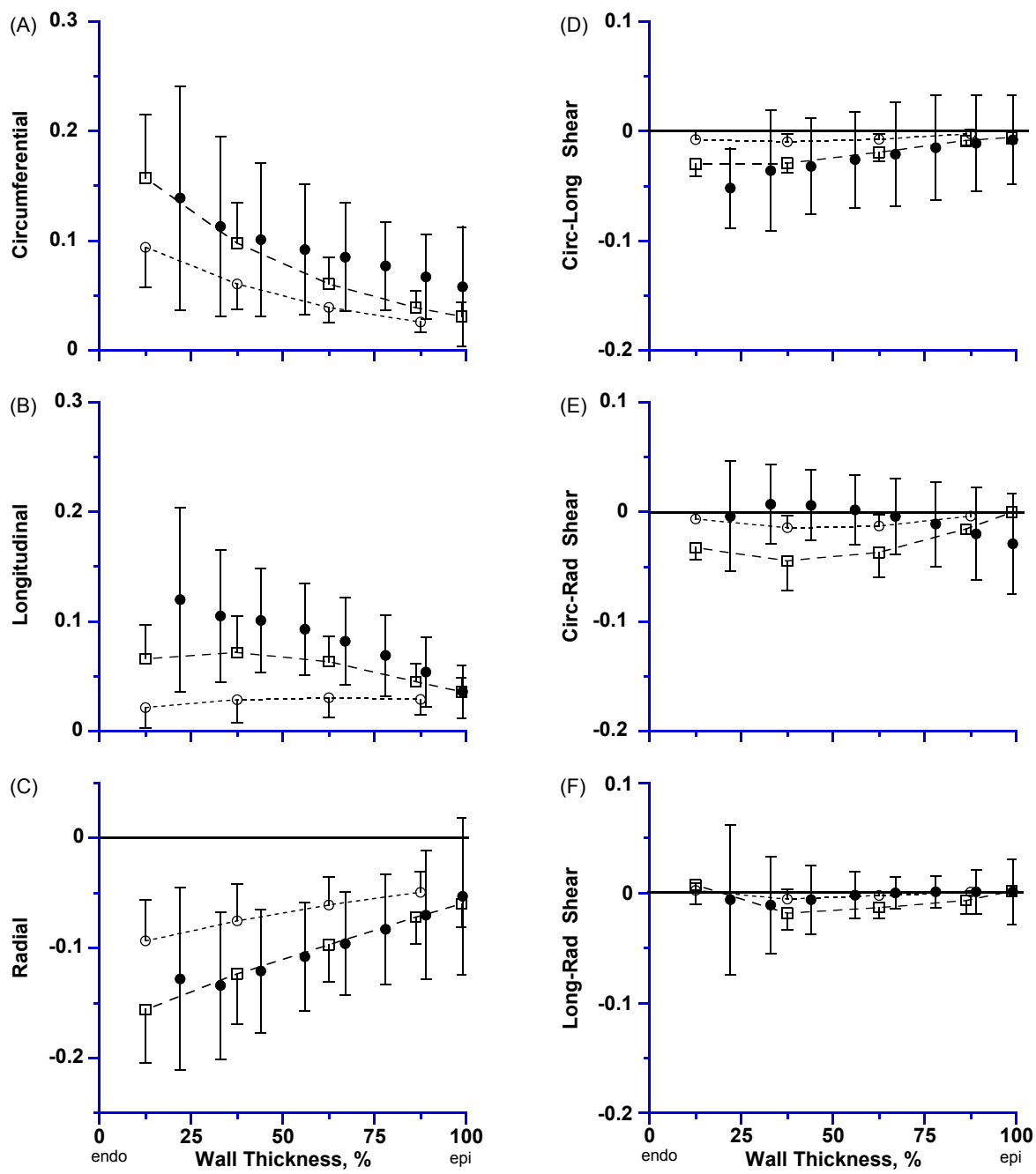


Figure 8, Okamoto et al.